Received March 18, 2022, accepted April 27, 2022, date of publication May 9, 2022, date of current version May 13, 2022.
Digital Object Identifier 10.1109/ACCESS.2022.3173754

Performance Evaluation of Short Packet Communications in NOMA VLC Systems With Imperfect CSI

GIANG N. TRAN, (Graduate Student Member, IEEE), AND SUNGHWAN KIM, (Member, IEEE)
Department of Electrical, Electronic, and Computer Engineering, University of Ulsan, Ulsan 44610, South Korea
Corresponding author: Sunghwan Kim (sungkim@ulsan.ac.kr)

This work was supported by the 2022 Research Fund of University of Ulsan.

ABSTRACT In this paper, we analyze and evaluate the impacts of imperfect channel state information (CSI) of the short packet communication (SPC) in a non-orthogonal multiple access (NOMA) visible light communication (VLC) system. We consider a downlink NOMA VLC system, in which one light emitting diode (LED) serves two single-photodiode users with the channel estimation error. To this end, we derive the closed-form expression for the block error rate (BLER) with imperfect CSI by using a Gaussian Chebyshev quadrature method, from which the expressions of reliability, latency, and throughput are carried out. Then, we compare the performance of the SPC in the NOMA VLC system to that of the OMA VLC system. The results show that the SPC-NOMA VLC system outperforms the SPC-OMA VLC system for all power allocation strategies and channel estimation errors. We examine the impact of the imperfect successive interference cancellation (SIC) at a near user and the impact of choosing LED semi-angle on the system throughput. Furthermore, we use the functional-iteration-based one-dimensional search method to get maximum throughput at the near user while guaranteeing a certain throughput at the far user.

INDEX TERMS Non-orthogonal multiple access (NOMA), short packet communication (SPC), visible light communication (VLC), ultra-reliable and low-latency communication (URLLC).

I. INTRODUCTION

The rapid growth of smartphones, tablets, and data-intensive applications, such as video streaming and virtual reality, has caused an explosive increase in global wireless data traffic on the order of a zettabyte [1]. The fifth generation (5G) and beyond are envisioned to provide high spectral efficiency, low latency, and massive connectivity [2]. Emerging technologies in 5G and beyond have been proposed to increase the data rate in future high-speed wireless communication systems such as network densification, massive multiple-input-multiple-output (MIMO) systems, millimeter wave (mmW) communications, and visible light communication (VLC) [3]. Along with the advancement and commercialization of light emitting diodes (LEDs), VLC has been of great interest in both academia and industry as a prospective technology for future wireless networks [3]. The significant advantage of VLC is the frequency spectrum on the order of THz (i.e., from 400 THz to 800 THz), which is equivalent to 10,000 times larger than the radio frequency (RF) system.

Ultra-reliable and low-latency communication (URLLC) is one of three key services in 5G networks [4]. URLLC applications include factory automation (FA), autonomous driving, remote surgery, smart grid automation, e-health, road safety, and Internet-of-Things (IoT) networks, which require reliability rate of 99.999% and very low latency on the order of sub-millisecond [5], [6]. In conventional wireless communication systems, the upper bound of the achievable rate has been approximated by Shannon's capacity theorem, and decoding error probability could be negligible, since the block-length of the packet size was assumed to be infinite [6]. In contrast, in URLLC, the packet size should be very low to support low-latency communication [5]. Inspired by this, short packet communication (SPC) was introduced to reduce transmission latency in the 5G and beyond [7]. The decoding error probability in SPC cannot be negligible due to the very low packet length [7]. Therefore, pioneering work [7] on SPC has showed that Shannon capacity cannot be directly applicable for the achievable

The associate editor coordinating the review of this manuscript and approving it for publication was Abderrezak Rachedi.

rate of the finite block-length transmission. The achievable rate in the finite block-length transmission of the SPC is expressed by a function of signal-to-noise ratio (SNR), block-length, and block error rate (BLER) of the system. Extensive research has been conducted on SPC in RF systems, such as quasi-static MIMO fading channels [8], broadcast channel [9], channel coding scheme [10], medium access control (MAC) channel [11], and mission-critical IoT applications [12]. The data transmission efficiency and throughput of spectrum sharing networks have been improved by using SPC [13]. In [14], the achievable rate was maximized with a long-term power for both additive white Gaussian noise (AWGN) and quasi-static channel, where the channel state information (CSI) was perfectly known at both transmitter and receiver. The authors of [15] proposed an energy-efficient packet scheduling for SPC, where the packet transmission power and code block-length were jointly optimized subject to delay constraints. In contrast, the research on the SPC in VLC systems has been conducted only rarely.

The multiple access techniques consist of two categories: orthogonal multiple access (OMA) and non-orthogonal multiple access (NOMA). OMA techniques include time division multiple access (TDMA), code division multiple access (CDMA), and frequency division multiple access (FDMA). In OMA techniques, users are supported in orthogonal resource (i.e., time slots, frequencies, and bandwidth) blocks to prevent interference between users. Therefore, the resource reuse in OMA schemes is inefficient for massive connectivity. On the other hand, NOMA can serve multiple users simultaneously in one resource block in the power domain. Thus, NOMA is a potential multiple access technique that could address the requirements of low latency, high connectivity, and high data rate for 5G wireless networks [16], [17]. In NOMA, signals for users are superposed in the power domain by superposition coding, and successive interference cancellation (SIC) is employed at the receiver to detect the signal. According to the NOMA principle, the power allocation for signals of users is based on the channel quality. The message signals for poor channel users gain higher power than those of strong channel users. Many aspects of NOMA in RF systems have been studied, such as wireless energy transfer [18], MIMO systems [19], multiple-antenna relaying networks [20], and cognitive radio [21]. Also, the implementation of NOMA in VLC systems has been studied to reduce latency and increase spectrum efficiency. The prior work on the NOMA in VLC system was reported in [22]. The authors of [23] evaluated the performance of NOMA in VLC systems with the assumption of perfect CSI and showed that NOMA increased the data rate of the VLC system in comparison to orthogonal frequency division multiple access (OFDMA). The bit-error-rate performance of NOMA in VLC systems was evaluated in [24] in the case of both perfect and imperfect CSI. The authors of [25] analyzed and evaluated the total system capacity of NOMA in MIMO VLC systems. Since the signals in VLC systems are real and non-negative, the implementation of NOMA in VLC systems should be considered carefully.

To satisfy the requirements of URLLC and to support massive connectivity, various studies have investigated the combination of SPC and NOMA in RF systems [7]– [15]. However, SPC in NOMA VLC systems has been studied only rarely due to fundamental differences in the signals. The aforementioned works focused on evaluating the data rate in NOMA VLC systems [22], [23], while the key requirements of URLLC (i.e., reliability and latency) were not discussed. Due to the noise in channels and hardware circuit design, the channel estimation in VLC systems is not always perfect in practical scenarios. To the best of our knowledge, the impacts of imperfect CSI in the SPC-NOMA VLC system were not evaluated. This motivates the investigation of imperfect CSI for NOMA VLC systems and URLLC applications. In this paper, we investigate the impacts of imperfect CSI in the SPC-NOMA VLC system in terms of reliability, latency, and throughput. Different from our previous work [26], we provide insightful evaluations of perfect/imperfect SIC and perfect/imperfect CSI for the practical designs of the SPC-NOMA VLC system. Moreover, we maximize the effective throughput at the near user while guanranteeing a specific constraint of the effective throughput at the far user, and the imperfect SIC is taken into account in the optimal design. We assume that two users are paired to support in one resource block. When there are more than two users, the proposed hybrid NOMA/OMA scheme in [27] is employed to support multiple user pairs. Therefore, this work is a significant step for massive connectivity scenarios. The contributions of this paper are summarized below.

- We derive the closed-form expression of the average BLER of the SPC-NOMA VLC system with imperfect CSI by assuming uniformly distributed users.
- We evaluate the performance of the imperfect CSI and imperfect SIC in the SPC-NOMA VLC system. To demonstrate the benefits of the SPC-NOMA VLC system, we compare NOMA versus OMA with SPC in the VLC system in terms of reliability, latency, and throughput.
- The impact of the LED semi-angle for imperfect SIC case is analyzed in the SPC-NOMA VLC system in term of system throughput.
- We derive the optimal system throughput design of the SPC-NOMA VLC system, where transmission rates and power allocation are two constraints. We maximize throughput of the near user while ensuring a certain throughput to the far user. We propose a simple and efficient method to obtain the transmission rate of the far user in the SPC-NOMA VLC system.

The remainder of this paper is organized as follows. In Section II, the preliminaries of imperfect CSI in the NOMA and OMA VLC systems are described, and the optimization problem is formulated. The average BLER performance is analyzed in Section III. In Section IV, the design of optimal system throughput is presented. In Section V, we present

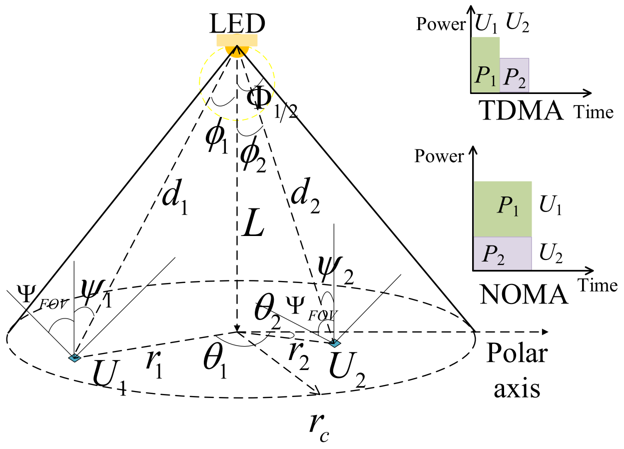

FIGURE 1. System model.

and discuss the analytical and simulation results. Finally, Section VI is the conclusion.

II. SYSTEM MODEL AND PRELIMINARY

A. SYSTEM MODEL

In this paper, we consider a downlink VLC system located in an indoor environment. The system model is depicted in Fig. 1, where one LED serves two single-photodiode users in the broadcast channel.[1] We assume that the system is located in a room where one LED is located on the ceiling to support users under the cell. The users are uniformly distributed in the circular area under the LED. Since the power of the diffusion component is much smaller than the line-of-sight (LOS) component, only the LOS component is considered in this work [23], [28]. The noise is additive white Gaussian with unit variance σ_n^2. The near user is defined as user in the cell center region and is denoted by U_2 with channel gain h_2. The far user is defined as user in the cell edge region and is denoted by U_1 with channel gain h_1 (i.e., $h_2 \geq h_1$). For intensity modulation and direct detection in the VLC system, the signals are processed to be real and non-negative by using Hermitian and adding DC bias at the LED [23], [28], [30]. In the NOMA VLC system, the LED simultaneously communicates with two users. In the OMA VLC, the TDMA is utilized to serve two users in orthogonal time-slots.

B. SPC IN VLC SYSTEMS

After applying Hermitian symmetry and adding DC bias [23], [28], [30], the message signal at the LED is given by

$$x_{\text{LED}} = \sqrt{P}s + V_{\text{LED}}, \tag{1}$$

where P, s, and V_{DC} are electrical power, message signal, and the DC bias to guarantee non-negative and unipolar signals, respectively.

At the receiver side, the signal is converted from optical power to electrical power by optical-to-electrical (O/E) conversion, and DC bias is eliminated. The received signal is represented by

$$y = \sqrt{P}hs + \mu_0, \tag{2}$$

where μ_0 is zero mean real-valued AWGN with σ_0^2. The received SNR γ at the user is given by

$$\gamma = \gamma_{\text{Tx}} h^2, \tag{3}$$

where γ_{Tx} is the transmitted SNR and is defined as $\gamma_{\text{Tx}} = P\sigma_0^2$. The BLER of SPC in VLC systems with a block-length N and a transmission rate R is approximated by [7], [26]

$$\varepsilon \approx Q\left(f\left(\gamma, R, N\right)\right), \tag{4}$$

where $f\left(\gamma, R, N\right) = \ln 2\sqrt{\frac{N}{0.5\left(1-(1+\gamma)^{-2}\right)}}$, $Q(\cdot)$ is Gaussian Q-function, with $Q\left(x\right) = \int_x^{\infty} e^{-t^2/2}\,dt$, and R is the ratio of the number of data bits k to the block-length N, $R = k/N$. The scaling factor 0.5 is due to Hermitian symmetry. The average BLER is calculated by

$$\begin{aligned}\bar{\varepsilon} &\approx E\Big\{Q\left(f\left(\gamma, R, N\right)\right)\Big\} \\ &= \int_{-\infty}^{\infty} Q\left(f\left(\gamma, R, N\right)\right) f_\gamma\left(x\right)\, dx,\end{aligned} \tag{5}$$

where $E\{.\}$ is expectation, and $E\{X\} = \int_{-\infty}^{\infty} x f_X\left(x\right)\, dx$.

C. NOMA TRANSMISSION IN VLC

In NOMA, the power allocation for message signals of each user is based on the channel quality. More power is allocated for users with lower channel gain, whereas less power is allocated for users with higher channel gain. After applying Hermitian and adding DC bias [23], [28], [30], the message signals are superposed at the LED. The transmitted signal at the LED is given by

$$x_{\text{LED}} = \sqrt{Pa_1}s_1 + \sqrt{Pa_2}s_2 + V_{\text{DC}}, \tag{6}$$

where s_1 and s_2 are message signals for U_1 and U_2, respectively, and a_1 and a_2 are power allocation coefficients for U_1 and U_2, respectively. According to NOMA principle, total power must satisfy $a_1 + a_2 = 1$ and $a_1 \geq a_2$.

At $U_i (i \in \{1, 2\})$, the SIC is performed to detect and remove the message signal of the higher channel user. After O/E conversion and DC bias removal, the message signal is

$$y_i = h_i\left(\sqrt{Pa_1}s_1 + \sqrt{Pa_2}s_2\right) + \mu_i, \tag{7}$$

where h_i is the channel gain between LED and U_i. At U_1, s_1 is directly decoded by treating s_2 as interference. The received SINR γ_{11} for U_1 to decode s_1 is

$$\gamma_{11} = \frac{a_1 P h_1^2}{a_2 P h_1^2 + \sigma_1^2}. \tag{8}$$

At U_2, the SIC is performed to detect and remove s_1, and then s_2 is detected and decoded. The received SINR γ_{21} in detecting s_1 at U_2 is

$$\gamma_{21} = \frac{a_1 P h_2^2}{a_2 P h_2^2 + \sigma_2^2}. \tag{9}$$

[1] According to the 3GPP-LTE Advanced, the two-user NOMA form is a fundamental block of NOMA [29]

After detecting and removing s_1, U_2 decodes s_2. The received SINR γ_{22} in detecting s_2 at U_2 is

$$\gamma_{22} = \frac{a_2 P h_2^2}{a_1 P h_2^2 \delta + \sigma_2^2}, \tag{10}$$

where $\delta \in [0, 1]$ is the interference factor caused by the imperfect SIC.

D. OMA TRANSMISSION IN VLC

In this paper, TDMA is considered as an OMA counterpart, which supports users in orthogonal time slots to avoid interference. The transmit signal to U_i in OMA is

$$x_{\mathrm{O}} = \sqrt{P a_i} s_i + V_{\mathrm{DC}}. \tag{11}$$

The received signal at U_i ($i \in \{1, 2\}$) after O/E conversion and removing DC bias is given by

$$y_i^{\mathrm{O}} = h_i \sqrt{P a_i} s_i + \mu_i. \tag{12}$$

The corresponding SNR in decoding s_i of U_i is expressed by

$$\gamma_i^{\mathrm{O}} = \frac{a_i P h_i^2}{\sigma_i^2}. \tag{13}$$

E. DISTRIBUTION FUNCTION OF THE RECEIVED SNR/SINR

According to NOMA principle, the power allocation strategy is based on the channel gains of users in VLC systems. The channel gain between U_i and LED is determined by [23], [28]

$$h_i = \frac{(m+1) A R_p}{2\pi d_i^2} \cos^m(\phi_i) T(\psi_i) g(\psi_i) \cos(\psi_i), \tag{14}$$

where the Lambertian emission order m is defined as $m = -\ln(2)/\ln(\cos(\Phi_{1/2}))$; $\Phi_{1/2}$ is the semi-angle of the LED; Ψ_{FOV} is the field-of-view (FOV) of the photodiode (PD); A is the PD area; R_p is the responsivity of the PD; d_i is the distance between U_i and LED; ϕ_i is the angle of irradiance; ψ_i is the angle of incidence; $T(\psi_i)$ is the optical filter gain; and $g(\psi_i)$ is the gain of the optical concentrator at the receiver, expressed by

$$g(\psi_i) = \begin{cases} \frac{n^2}{\sin^2(\Psi_{\mathrm{FOV}})}, & 0 \le \psi_i \le \Psi_{\mathrm{FOV}}, \\ 0, & \psi_i > \Psi_{\mathrm{FOV}}, \end{cases} \tag{15}$$

where $n \in [1, 2]$ represents the refractive index of the optical concentrator. In Fig. 1, user position follows a uniform distribution and is located at the angle θ_i and position r_i in the polar axis. The vertical distance from the LED to the circular plane is L. The radius of the circular area is denoted by r_c. The distance between LED and U_i, the angle of irradiance, and the angle of incidence are calculated by $d_i = \sqrt{r_i^2 + L^2}$, $\cos(\phi_i) = L/\sqrt{r_i^2 + L^2}$, $\cos(\psi_i) = L/\sqrt{d_i^2 + L^2}$, respectively. Since $r_i \in [0, r_c]$, the channel gain is bounded as $h_i \in [h_{\min}, h_{\max}]$, and $h_{\min}$ and $h_{\max}$ are given as

$$h_{\min} = \sqrt{\left(\mathcal{C}\,(m+1)\,L^{m+1}\right)^2 / \left(r_c^2 + L^2\right)^{(m+3)}} \tag{16}$$

and

$$h_{\max} = \sqrt{\left(\mathcal{C}\,(m+1)\,L^{m+1}\right)^2 / L^{2(m+3)}}, \tag{17}$$

where $\mathcal{C} = \frac{1}{2\pi} A T(\psi_i) g(\psi_i)$. The probability density function (PDF) of the uniformly distributed user position in the circular area is $f_{r_i}(r) = 2r/r_c^2$. The unordered PDF of the received SNR at U_i is given by [23]

$$f_{\gamma_i}^{\gamma}(x) = \frac{1}{r_c^2} \frac{1}{m+3} \left(\mathcal{C}\,(m+1)\,L^{m+1}\right)^{\frac{2}{m+3}} \left(\frac{1}{\gamma_{\mathrm{Tx}}}\right)^{-\frac{1}{m+3}} \times x^{-\frac{1}{m+3}-1}, \tag{18}$$

where $\gamma_i = \gamma_{\mathrm{Tx}} h_i^2$. Since $h_i \in [h_{\min}, h_{\max}]$, then $\gamma_i \in [\gamma_{\min}, \gamma_{\max}] = [\gamma_{\mathrm{Tx}} h_{\min}^2, \gamma_{\mathrm{Tx}} h_{\max}^2]$. The unordered cumulative distribution function (CDF) of the received SNR at U_i is derived by integrating (18) over $[\gamma_{\min}, \gamma_{\max}]$, and expressed as

$$F_{\gamma_i}^{\gamma}(x) = -\frac{1}{r_c^2} \frac{1}{m+3} \left(\mathcal{C}(m+1)L^{m+1}\right)^{\frac{2}{m+3}} \times \left(\frac{1}{\gamma_{\mathrm{Tx}}}\right)^{-\frac{1}{m+3}} x^{-\frac{1}{m+3}} + \frac{L^2}{r_c^2} + 1. \tag{19}$$

Due to sorting the channel gains for power allocation strategy in NOMA, the ordered statistics can be applied [26], [31, Chapter 2]. The ordered PDF of the SNR at U_i is given by

$$\begin{aligned} f_{\gamma_i}(x) &= \frac{2!}{(2-i)!(i-1)!} \left(F_{\gamma_i}^{\gamma}(x)\right)^{i-1} \left(1 - F_{\gamma_i}^{\gamma}(x)\right)^{2-i} \times f_{\gamma_i}^{\gamma}(x) \\ &= \frac{\omega}{m+3} \frac{2!}{(2-i)!(i-1)!} \left(-\omega x^{-\frac{1}{m+3}} + \frac{L^2}{r_c^2} + 1\right)^{i-1} \\ &\quad \times \left(\omega x^{-\frac{1}{m+3}} - \frac{L^2}{r_c^2}\right)^{2-i} x^{-\frac{1}{m+3}-1}, \end{aligned} \tag{20}$$

where $\omega = \frac{1}{r_c^2} \left(\mathcal{C}(m+1)L^{m+1}\right)^{\frac{2}{m+3}} \left(\frac{1}{\gamma_{\mathrm{Tx}}}\right)^{-\frac{1}{m+3}}$.

F. IMPERFECT CSI IN VLC SYSTEMS

It is assumed that the estimated channel value $\hat{h}_i$ between U_i and the LED is obtained by using the minimum mean square error (MMSE) estimation model, and the channel estimation error e_i is introduced by the noise in the downlink and uplink channels and the quantization errors from the imperfect analog-to-digital and digital-to-analog conversions [32]. Then, the channel value h_i between U_i and LED is expressed as

$$h_i = \hat{h}_i + e_i, \tag{21}$$

where e_i has a Gaussian distribution with zero-mean and variance $\sigma_{e_i}^2$, i.e., $e_i \sim \mathcal{N}\left(0, \sigma_{e_i}^2\right)$. Then, the received signal at U_i in (7) is given by

$$y_i = \left(\hat{h}_i + e_i\right)\left(\sqrt{P a_1} s_1 + \sqrt{P a_2} s_2\right) + \mu_i. \tag{22}$$

The SINRs during decoding message signal at each user in the NOMA VLC system with imperfect CSI are expressed by

$$\hat{\gamma}_{11} = \frac{a_1 P\hat{h}_1^2}{a_2 P\hat{h}_1^2 + P\sigma_{e_1}^2 + \sigma_1^2}, \tag{23}$$

$$\hat{\gamma}_{21} = \frac{a_1 P\hat{h}_2^2}{a_2 P\hat{h}_2^2 + P\sigma_{e_2}^2 + \sigma_2^2}, \tag{24}$$

$$\hat{\gamma}_{22} = \frac{a_2 P\hat{h}_2^2}{a_1 P\hat{h}_2^2\delta + P\sigma_{e_2}^2 + \sigma_2^2}. \tag{25}$$

The corresponding SINR of each user in the OMA VLC system with imperfect CSI is given by

$$\hat{\gamma}_i = \frac{a_i P\hat{h}_i^2}{P\sigma_{e_i}^2 + \sigma_i^2}. \tag{26}$$

G. RELIABILITY, LATENCY, AND THROUGHPUT CALCULATION

Reliability of a packet is defined as the probability that a packet is successfully decoded at the receiver, given by

$$\mathcal{R} = (1 - \varepsilon_i)\, 100\%, \tag{27}$$

where the BLER ε_i is calculated by (4). The latency is the average delay in the transmission from the LED to U_i and decoding time at U_i, given by

$$\mathcal{L} = \frac{N\mathcal{J}_S}{(1 - \varepsilon_i)}, \tag{28}$$

where $\mathcal{J}_s$ is the block duration. The effective throughput at U_i represents the number of correct information bits per transmission, given by

$$T_i = \frac{N_i}{N} R_i (1 - \epsilon_i), \tag{29}$$

where N_i is the block-length allocated for U_i and R_i is the transmission rate at U_i.

H. OPTIMIZATION PROBLEM

In our model, the LED serves U_1 and U_2 simultaneously. The block-length N is transmitted to ensure the reliability of the system. Since the NOMA system transmits signals to U_1 and U_2 simultaneously, we have $N_1 = N_2 = N$. The goal of our optimization is to get the maximum sum throughput while guaranteeing a specific throughput constraint T_0 to the far user (U_1). This means that the throughput at U_2 is maximized with a specific constraint of throughput at U_1 subject to the total power constraint. The optimization problem is mathematically formulated as

$$\max_{\Delta} \quad T_2 \tag{30a}$$

$$a_1 + a_2 = 1, \tag{30b}$$

$$T_1 \geq T_0, \tag{30c}$$

where $\Delta = \{R_1, R_2, a_1, a_2\}$ is the variable set to be determined at the LED for the NOMA-VLC system.

III. PERFORMANCE EVALUATION

In this section, the effects of imperfect CSI on the BLER are discussed.

A. AVERAGE BLER OF SPC-NOMA VLC

The average BLER at U_i is given by

$$\begin{aligned}\bar{\varepsilon}_i &\approx E\left\{Q\left(f\left(\gamma_i, R_i, N_i\right)\right)\right\} \\ &= \int_{-\infty}^{\infty} Q\left(f\left(\gamma_i, R_i, N_i\right)\right) f_{\gamma_i}(x)dx.\end{aligned} \tag{31}$$

Since $\gamma_i \in [\gamma_{i,\min}, \gamma_{i,\max}]$, the average BLER at U_i is expressed by

$$\bar{\varepsilon}_i = \int_{\gamma_{i,\min}}^{\gamma_{i,\max}} Q\left(f\left(\gamma_i, R_i, N_i\right)\right) f_{\gamma_i}(x)dx. \tag{32}$$

Since there exists a Q-function, the integral in (32) cannot be derived directly in closed form. The Gaussian quadrature is used to approximate (32) as [33, Table 25.4]

$$\begin{aligned}\bar{\varepsilon}_i \triangleq g\left(\gamma_{i,\max}, \gamma_{i,\min}, N_i, R_i\right) &= \mathcal{U}_i \sum_{w=1}^{\mathcal{W}} \frac{\pi}{\mathcal{W}} \sqrt{1 - \zeta^2} \\ &\times Q\left(\frac{\ln 2\sqrt{N_i}\left(0.5\log_2\left(1 + \mathcal{U}_i\zeta + \mathcal{V}_i\right) - R_i\right)}{\sqrt{0.5\left(1 - \left(1 + \mathcal{U}_i\zeta + \mathcal{V}_i\right)^{-2}\right)}}\right) \\ &\times f_{\gamma_i}\left(\mathcal{U}_i\zeta + \mathcal{V}_i\right),\end{aligned} \tag{33}$$

where $\mathcal{W}$ is the complexity-accuracy trade-off parameter, $\zeta = \cos\left(\frac{(2w-1)\pi}{2\mathcal{W}}\right)$, $\mathcal{U}_i = \frac{\gamma_{i,\max} - \gamma_{i,\min}}{2}$, and $\mathcal{V}_i = \frac{\gamma_{i,\max} + \gamma_{i,\min}}{2}$.

B. BLER OF IMPERFECT CSI IN SPC-NOMA VLC

1) SIGNAL PROCESSING AT U_1

Since U_1 is the priori user in the two-user NOMA system, the message s_1 is directly decoded by treating s_2 as interference. The SINR in decoding s_1 due to imperfect CSI is given as

$$\hat{\gamma}_{11} = \frac{a_1\hat{\gamma}_1}{a_2\hat{\gamma}_1 + \gamma_{\text{Tx}}\sigma_{e_1}^2 + 1}. \tag{34}$$

The ordered PDF of $\hat{\gamma}_{11}$ is derived to get the average BLER of s_1. From (21) and (22), the unordered CDF and unordered PDF of $\hat{\gamma}_{11}$ are given as

$$\begin{aligned}F_{\hat{\gamma}_{11}}^{\hat{\gamma}}(x) = -\omega\left(\gamma_{\text{Tx}}\sigma_{e_1}^2 + 1\right)^{-\frac{1}{m+3}} &\left(\frac{x}{a_1 - a_2 x}\right)^{-\frac{1}{m+3}} \\ &+ \frac{L^2}{r_c^2} + 1\end{aligned} \tag{35}$$

and

$$\begin{aligned}f_{\hat{\gamma}_{11}}^{\hat{\gamma}}(x) = \frac{1}{m+3}\omega\left(\gamma_{\text{Tx}}\sigma_{e_1}^2 + 1\right)^{-\frac{1}{m+3}} &\left(\frac{x}{a_1 - a_2 x}\right)^{-\frac{m+4}{m+3}} \\ &\times \frac{a_1}{(a_1 - a_2 x)^2}.\end{aligned} \tag{36}$$

The ordered PDF of $\hat{\gamma}_{11}$ is given by

$$f_{\hat{\gamma}_{11}}(x) = 2\left(1 - F_{\hat{\gamma}_{11}}^{\hat{\gamma}}(x)\right) f_{\hat{\gamma}_{11}}^{\hat{\gamma}}(x). \tag{37}$$

Since $\hat{\gamma}_1 \in [\hat{\gamma}_{\min}, \hat{\gamma}_{\max}]$, then $\hat{\gamma}_{11} \in [\hat{\gamma}_{11,\min}, \hat{\gamma}_{11,\max}]$ according to (34). From (33), (34) and (37), the average BLER at U_1 is written by

$$\bar{\varepsilon}_1 = g\left(\hat{\gamma}_{11,\max}, \hat{\gamma}_{11,\min}, N, R_1\right). \tag{38}$$

2) SIGNAL PROCESSING AT U_2

To decode signal s_2 for U_2, s_1 is detected and subtracted by treating s_2 as interference. The decoding SINR of s_1 due to imperfect CSI at U_2 is written by

$$\hat{\gamma}_{21} = \frac{a_1\hat{\gamma}_2}{a_2\hat{\gamma}_2 + \gamma_{\mathrm{Tx}}\sigma_{e_2}^2 + 1}. \tag{39}$$

The unordered CDF and unordered PDF of $\hat{\gamma}_{21}$ are

$$F_{\hat{\gamma}_{21}}^{\hat{\gamma}}(x) = -\omega\left(\gamma_{\mathrm{Tx}}\sigma_{e_2}^2 + 1\right)^{-\frac{1}{m+3}}\left(\frac{x}{a_1 - a_2x}\right)^{-\frac{1}{m+3}} + \frac{L^2}{r_c^2} + 1 \tag{40}$$

and

$$f_{\hat{\gamma}_{21}}^{\hat{\gamma}}(x) = \frac{1}{m+3}\omega\left(\gamma_{\mathrm{Tx}}\sigma_{e_2}^2 + 1\right)^{-\frac{1}{m+3}}\left(\frac{x}{a_1 - a_2x}\right)^{-\frac{m+4}{m+3}} \times \frac{a_1}{(a_1 - a_2x)^2}. \tag{41}$$

The ordered PDF of $\hat{\gamma}_{21}$ is

$$f_{\hat{\gamma}_{21}}(x) = 2F_{\hat{\gamma}_{21}}^{\hat{\gamma}}(x)f_{\hat{\gamma}_{21}}^{\hat{\gamma}}(x). \tag{42}$$

Since $\hat{\gamma}_2 \in [\hat{\gamma}_{\min}, \hat{\gamma}_{\max}]$, then $\hat{\gamma}_{21} \in [\hat{\gamma}_{21,\min}, \hat{\gamma}_{21,\max}]$ according to (39). From (33), (39), and (42), the average BLER in decoding s_1 at U_2 is given by

$$\bar{\varepsilon}_{21} = g\left(\hat{\gamma}_{21,\max}, \hat{\gamma}_{21,\min}, N, R_1\right). \tag{43}$$

In practical hardware design, the SIC is not always perfect. Therefore, the SIC cannot totally decode and remove s_1, and s_1 becomes the residual interference in decoding s_2 at U_2. The decoding SINR of s_2 due to imperfect CSI at U_2 is written as

$$\hat{\gamma}_{22} = \frac{a_2\hat{\gamma}_2}{a_1\hat{\gamma}_2\delta + \gamma_{\mathrm{Tx}}\sigma_{e_2}^2 + 1}. \tag{44}$$

The unordered CDF and unordered PDF of $\hat{\gamma}_{22}$ are

$$F_{\hat{\gamma}_{22}}^{\hat{\gamma}}(x) = -\omega\left(\gamma_{\mathrm{Tx}}\sigma_{e_2}^2 + 1\right)^{-\frac{1}{m+3}}\left(\frac{x}{a_2 - a_1\delta x}\right)^{-\frac{1}{m+3}} + \frac{L^2}{r_c^2} + 1 \tag{45}$$

and

$$f_{\hat{\gamma}_{22}}^{\hat{\gamma}}(x) = \frac{1}{m+3}\omega\left(\gamma_{\mathrm{Tx}}\sigma_{e_2}^2 + 1\right)^{-\frac{1}{m+3}}\left(\frac{x}{a_2 - a_1\delta x}\right)^{-\frac{m+4}{m+3}} \times \frac{a_2}{(a_2 - a_1\delta x)^2}. \tag{46}$$

The ordered PDF of $\hat{\gamma}_{22}$ is

$$f_{\hat{\gamma}_{22}}(x) = 2F_{\hat{\gamma}_{22}}^{\hat{\gamma}}(x)f_{\hat{\gamma}_{22}}^{\hat{\gamma}}(x). \tag{47}$$

Since $\hat{\gamma}_2 \in [\hat{\gamma}_{\min}, \hat{\gamma}_{\max}]$, then $\hat{\gamma}_{22} \in [\hat{\gamma}_{22,\min}, \hat{\gamma}_{22,\max}]$ according to (44). From (33), (44), and (47), the average BLER in decoding s_2 at U_2 is given by

$$\bar{\varepsilon}_{22} = g\left(\hat{\gamma}_{22,\max}, \hat{\gamma}_{22,\min}, N, R_2\right). \tag{48}$$

The overall average error probability of s_2 at U_2 is

$$\bar{\varepsilon}_2 = \bar{\varepsilon}_{22}\left(1 - \bar{\varepsilon}_{21}\right) + \bar{\varepsilon}_{21}. \tag{49}$$

C. BLER OF IMPERFECT CSI IN SPC-OMA VLC

In the OMA, the users are supported in orthogonal resource blocks to avoid the interference. The block-lengths for U_1 and U_2 are N_1 and N_2, respectively, and $N_1 + N_2 = N$. The power allocation coefficients are determined by order of the channel magnitude. The SNR in decoding s_i at U_i is given by

$$\hat{\gamma}_i^{\mathrm{O}} = \frac{a_i\hat{\gamma}_i}{\gamma_{\mathrm{Tx}}\sigma_{e_i}^2 + 1}. \tag{50}$$

The BLER of s_i at U_i is $\varepsilon_i^{\mathrm{O}} = Q\left(f\left(\gamma_i^{\mathrm{O}}, R_i, N_i\right)\right)$. The unordered PDF and CDF of γ_i^{O} are

$$F_{\hat{\gamma}_i^{\mathrm{O}}}^{\hat{\gamma}}(x) = -\omega\left(\frac{\gamma_{\mathrm{Tx}}\sigma_{e_i}^2 + 1}{a_i}\right)^{-\frac{1}{m+3}} x^{-\frac{1}{m+3}} + \frac{L^2}{r_c^2} + 1 \tag{51}$$

and

$$f_{\hat{\gamma}_i^{\mathrm{O}}}^{\hat{\gamma}}(x) = \frac{1}{m+3}\omega\left(\frac{\gamma_{\mathrm{Tx}}\sigma_{e_i}^2 + 1}{a_i}\right)^{-\frac{1}{m+3}} x^{-\frac{m+4}{m+3}}. \tag{52}$$

The unordered PDF of $\hat{\gamma}_i^{\mathrm{O}}$ is

$$f_{\hat{\gamma}_i^{\mathrm{O}}}(x) = \frac{2!}{(2-i)!(i-1)!}\left(F_{\hat{\gamma}_i^{\mathrm{O}}}^{\hat{\gamma}}(x)\right)^{i-1} \times \left(1 - F_{\hat{\gamma}_i^{\mathrm{O}}}^{\hat{\gamma}}(x)\right)^{2-i} f_{\hat{\gamma}_i^{\mathrm{O}}}^{\hat{\gamma}}(x). \tag{53}$$

Since $\hat{\gamma}_i \in [\hat{\gamma}_{\min}, \hat{\gamma}_{\max}]$, then $\hat{\gamma}_i^{\mathrm{O}} \in [\hat{\gamma}_{i,\min}^{\mathrm{O}}, \hat{\gamma}_{i,\max}^{\mathrm{O}}]$ according to (50). The average BLER in decoding s_i at U_i is given by

$$\bar{\varepsilon}_i^{\mathrm{O}} = g\left(\hat{\gamma}_{i,\max}^{\mathrm{O}}, \hat{\gamma}_{i,\min}^{\mathrm{O}}, N_i, R_i\right). \tag{54}$$

IV. OPTIMAL SYSTEM THROUGHPUT DESIGN

In this section, we propose the design of transmission rates and power allocation strategy to solve the optimization in (30). To facilitate the optimal design, we examine the two constraints in (30b) and (30c). Since the perfect SIC cannot always be ensured, we take into account the SIC failure (i.e., $\delta = 1$) at U_2 in the optimal system throughput design.[2] We present the analysis of the optimal system throughput design below.

Since U_1 directly decodes its own message signal, then from (4) and (35), the decoding error probability at U_1 is

$$\varepsilon_1 = Q\left(f\left(\hat{\gamma}_{11}, R_1, N\right)\right). \tag{55}$$

[2]In practical scenarios, it is difficult to determine an imperfect SIC value due to the circuit design and error propagation. Therefore, the SIC failure is considered for the imperfect SIC case in the optimal throughput design.

The effective throughput at U_1 is

$$T_1 = R_1\left(1-\varepsilon_1\right). \tag{56}$$

At U_2, SIC is performed to decode and subtract s_1 first, and then s_2 is decoded. From (4) and (39), the decoding error probability of s_1 at U_2 is given by

$$\varepsilon_{21} = Q\left(f\left(\hat{\gamma}_{21}, R_1, N\right)\right). \tag{57}$$

This demonstrates that s_1 can be accurately removed at U_2 with probability $1-\varepsilon_{21}$. If U_2 successfully decodes s_1, it decodes its own signal s_2. The corresponding SINR of s_2 at U_2 is given by

$$\hat{\gamma}_{22} = \frac{a_2\hat{\gamma}_2}{\gamma_{\mathrm{Tx}}\sigma_{e_2}^2+1}. \tag{58}$$

From (4) and (58), the decoding error probability of s_2 at U_2 is given by

$$\varepsilon_{22} = Q\left(f\left(\hat{\gamma}_{22}, R_2, N\right)\right). \tag{59}$$

The overall decoding error probability at U_2 with perfect SIC is

$$\varepsilon_2 = \varepsilon_{22}\left(1-\varepsilon_{21}\right)+\varepsilon_{21}. \tag{60}$$

The effective throughput at U_2 is given by

$$T_2 = R_2\left(1-\varepsilon_2\right). \tag{61}$$

However, if SIC is failed, s_1 is interference in decoding s_2 at U_2, and the probability of the SIC failure is ε_{21}. Therefore, the corresponding SINR of s_2 at U_2 is

$$\hat{\gamma}_{22}' = \frac{a_2\hat{\gamma}_2}{a_1\hat{\gamma}_2+\gamma_{\mathrm{Tx}}\sigma_{e_2}^2+1}. \tag{62}$$

From (4) and (62), the corresponding error probability of s_2 at U_2 is given by

$$\varepsilon_{22}' = Q\left(f\left(\hat{\gamma}_{22}', R_2, N\right)\right). \tag{63}$$

According to [34], the decoding error probability at U_2 has a Bernoulli distribution property. When the SIC is successful with probability $1-\varepsilon_{21}$, the error probability is ε_{22}. When the SIC fails with probability ε_{21}, the error probability is ε_{22}'. Therefore, the overall decoding error probability of s_2 at U_2 is

$$\varepsilon_2' = \varepsilon_{22}\left(1-\varepsilon_{21}\right)+\varepsilon_{21}\varepsilon_{22}'. \tag{64}$$

The effective throughput at U_2 is

$$T_2' = R_2\left(1-\varepsilon_2'\right). \tag{65}$$

Proposition 1: The error probability in (4) *is a decreasing function with respect to the corresponding SNR/SINR, proved in [26, Proposition 1].*

Proposition 2: The error probability in (4) *is an increasing function with the corresponding transmission rate R_i, provided in [26, Proposition 2].*

In the optimal design, the total power is fully consumed to transmit signals to U_1 and U_2. According to (56), T_1 is an increasing function with respect to a_1, whereas T_2 and T_2' are not increasing functions with respect to a_2. Thus, it is a challenge to determine the optimal power allocation strategy, since $a_1 + a_2 = 1$. To address the optimization problem, we detail the steps of the optimal design in the SPC-NOMA-VLC system with imperfect CSI as follows.

Step 1: Find R_1 with respect to the possible values of a_1.

Since U_1 directly decodes s_1, R_1 and R_2 are independent. To obtain the value of R_1, we examine the monotonicity and concavity of T_1 with respect to R_1.

Lemma 1: T_1 is not an increasing function with R_1 but is concave with R_1.

Proof: Please see Appendix A. □

According to Lemma 1, there exists an optimal R_1 where $T_1(R_1) = T_0$ with a feasible value of a_1. From Lemma 1, two values of R_1 can provide $T_1(R_1) = T_0$ for each feasible a_1. Following (61), (65), and Proposition 2, T_2 is a decreasing function with respect to R_1. Therefore, the smaller R_1 can provide the maximum total throughput of the system (i.e., $\frac{\partial T_1}{\partial R_1} \geq 0$), denoted by R_1^{opt}. Since T_1 includes a special Q-function, R_1 cannot be directly derived in the closed form.

Proposition 3: By using the functional iteration method, R_1 can be derived as

$$R_1 := \mathcal{T}\left(R_1\right) = \frac{T_0}{1-Q\left(f\left(\hat{\gamma}_{11}, R_1, N\right)\right)}. \tag{66}$$

Proof: Please see Appendix B. □

Step 2. Find the value of R_2 with the derived a_1, a_2, and R_1.

Lemma 2: The throughput at U_2 is a concave function with R_2.

Proof: Please see Appendix C. □

Let $R' = 0.5\log_2\left(1+\hat{\gamma}_{22}'\right)$ and $\tilde{R} = 0.5\log_2\left(1+\hat{\gamma}_{22}\right)$. According to Appendix C, the value of optimal R_2 that maximizes T_2 is given by

$$R_2^{\mathrm{opt}} = \begin{cases} \hat{R}_2^{\max}, & \text{if } 0 \leq R_2 \leq R', \\ \bar{R}_2^{\max}, & \text{if } R' < R_2 \leq \tilde{R}, \end{cases} \tag{67}$$

where $\hat{R}_2^{\max}$ maximizes T_2' and $\bar{R}_2^{\max}$ maximizes T_2. Since T_2' and T_2 are concave functions with R_2 on the reasonable interval, $\hat{R}_2^{\max}$ and $\bar{R}_2^{\max}$ can be derived by the golden search method.

Step 3. Find optimal throughput at U_2 and optimal power allocation strategy.

To find the set of feasible power allocation, we use one-dimensional numerical search method with a_1, since $0.5 \leq a_1 \leq 1$. The value of R_1 is derived by Step 1. In Step 2, R_2 is obtained with $a_2 = 1 - a_1$. The set of throughputs at U_2 is determined. These steps are repeated until the maximum throughput at U_2 is found, and then the corresponding optimal a_2 is carried out. Finally, the set of optimal values a_1, a_2, R_1, and R_2 can be obtained. The proposed optimal algorithm is presented in **Algorithm 1**.

The complexity of the functional-iteration-based one-dimensional search method is $\mathcal{O}\left(N_P\left(N_f+N_g\right)\right)$, where N_P is the size of input power allocation coefficients, $N_f = \left\lceil\frac{\log_2(1/\alpha)}{\log_2(1/(1-\alpha))}\right\rceil$ is the complexity of the functional iteration

Algorithm 1 Optimization of the power allocation and transmission rates.

Input: Initialize T_0, $a_1 = a_1^b : \tau : 1$ step size of power allocation τ, tolerance error of R_1 α, tolerance error of R_2 β, initial guess of R_1 $R_{1,g}$, $R_{2,min}$, $R_{2,max}$, step size for golden search procedure $\Lambda = \frac{\sqrt{5}-1}{2}$, and $T_{2,max} = 0$.
Output: a_1^{opt}, a_2^{opt}, R_1^{opt}, R_2^{opt}
for $i \leftarrow 1$ *to length*(a_1) **do**
    `// Obtain` R_1 `by functional iteration method`
    Calculate: $R_1 \leftarrow \mathcal{T}\left(R_{1,g}, a_1(i)\right)$ according to (66)
    while $\left|R_{1,g} - R_1\right| \leq \alpha$ **do**
        Update: $R_{1,g} \leftarrow \mathcal{T}\left(R_1, a_1(i)\right)$
    Set: $R_1 \leftarrow R_{1,g}$
    `// Obtain` R_2 `by Golden search method`
    Calculate:
    $R_{2,1} \leftarrow R_{2,max} - \left(R_{2,max} - R_{2,min}\right)\Lambda$ and
    $R_{2,2} \leftarrow R_{2,min} + \left(R_{2,max} - R_{2,min}\right)\Lambda$.
    while $\left|R_{2,max} - R_{2,min}\right| \leq \beta$ **do**
        Update: $T_{2,1} \leftarrow T_2\left(R_{2,1}\right)$ from (67)
        Update: $T_{2,2} \leftarrow T_2\left(R_{2,2}\right)$ from (67)
        if $T_{2,1} > T_{2,2}$ **then**
            Update: $R_{2,max} \leftarrow R_{2,2}$
        else
            Update: $R_{2,min} \leftarrow R_{2,1}$
    Set: $R_2 \leftarrow \left(R_{2,max} + R_{2,min}\right)/2$
    `// Obtain optimal set`
    Set: $T_{2,samp} \leftarrow T_2(R_2)$
    if $T_{2,samp} > T_{2,max}$ **then**
        Update: $T_{2,max} \leftarrow T_{2,samp}$
        Update: $R_1^{opt} \leftarrow R_1$
        Update: $R_2^{opt} \leftarrow R_2$
        Update: $a_1^{opt} \leftarrow a_1(i)$
        Update: $a_2^{opt} \leftarrow 1 - a_2^{opt}$

method with the tolerance error α [36], and $N_g = \log_2 \frac{1}{\beta}$ is the complexity of the golden search method with the tolerance error β [37].

V. NUMERICAL RESULTS AND DISCUSSION

In this section, we present the derived analytical results, which are verified by Monte Carlo simulations and provide optimal results. The results show that the simulation results match well with analytical results formulated in Section III. The performance comparisons between SPC in NOMA versus OMA VLC systems include: (i) the BLER performance as a function of transmit SNR with various power allocation strategies, (ii) the BLER performance as a function of the channel estimation error, (iii) the throughput as a function of transmit SNR, and (iv) reliability and latency as a function of the block-length. The impact of imperfect SIC is analyzed. The choice of the LED semi-angle with imperfect CSI is analyzed with various values of channel gain and transmit SNR. We present the optimal result based on given estimated channel gains. The simulation parameters are listed in Table 1. Since the NOMA scheme supports two users simultaneously, we choose the block-length $N_1 = N_2 = N = 200$. In the OMA counterpart, TDMA serves each user in one time-slot with $N_1 = N_2 = N/2 = 100$. The number of data bits for each user is $k_1 = k_2 = 80$ bits. The power allocation coefficients are $a_1 = 0.8$ and $a_2 = 0.2$. In the figures, we denote 'Ana.' and 'Sim.' as analytical results and simulation results, respectively.

TABLE 1. Simulation parameters.

Parameter name	Notation	Value
Vertical distance from LED to circular plane	L	2.5 m
Radius of the circular plane	r_c	3.5 m
LED semi-angle	$\Phi_{1/2}$	60°
PD FOV	Ψ_{FOV}	60°
PD responsibility	R_p	0.4 A/W
PD detection area	A	1 cm^2
Reflective index	n	1.5
Optical filter gain	T	1
Block duration	$\mathcal{J}_s$	0.1 μs

Fig. 2 presents a comparison of the average BLER between the SPC-NOMA VLC system and the SPC-OMA VLC system with various power allocation strategies as a function of the transmit SNR. The results show that the simulation results match well with the analytical results. The BLER of U_1 in the SPC-NOMA VLC system is higher than that of U_1 in the SPC-OMA VLC system with $a_1 = 0.6$, since the power allocation for message signals of U_2 makes interference in decoding s_1 at U_1 of the NOMA system. The BLERs of all users in the SPC-NOMA VLC system are lower than those of all users in the SPC-OMA VLC system with $a_1 = 0.7$, $a_1 = 0.8$, and $a_1 = 0.9$ in the cases of imperfect CSI and perfect SIC. In the SPC-OMA VLC system, the BLER of U_2 is better than that of U_1 with value of transmit SNR less than 138 dB due to low transmit power and effect of the imperfect CSI. However, the BLER of U_1 is always lower than that of U_2 with transmit SNR larger than 138 dB, since higher power is allocated to signals of U_1 and there is no interference caused by signals of another user. In the SPC-NOMA VLC system, the BLER of U_1 is higher than that of U_2 with $a_1 = 0.6$ and $a_1 = 0.7$ due to interference of the power allocation for the message of U_2 in decoding s_1. The BLER of the U_1 is lower than that of U_2 when the power is boosted to U_1 (i.e., $a_1 = 0.8$ and $a_1 = 0.9$). The BLER performance of the SPC-NOMA VLC system requires less power to get the error floor than that of the SPC-OMA VLC system (i.e., 150 dB in NOMA system, and 155 dB in OMA system with all power allocation strategies). It can be concluded that the BLER of U_1 (far user) is improved when the power allocation for U_1 is boosted.

Fig. 3 illustrates that the BLER of the perfect CSI scenario (i.e., $\sigma_e^2 = 0$) outperforms those of the imperfect CSI

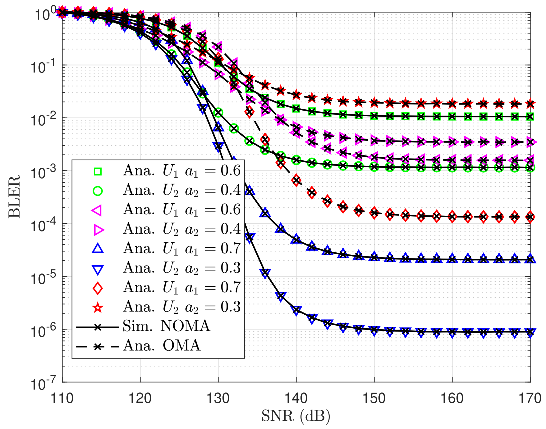

(a)

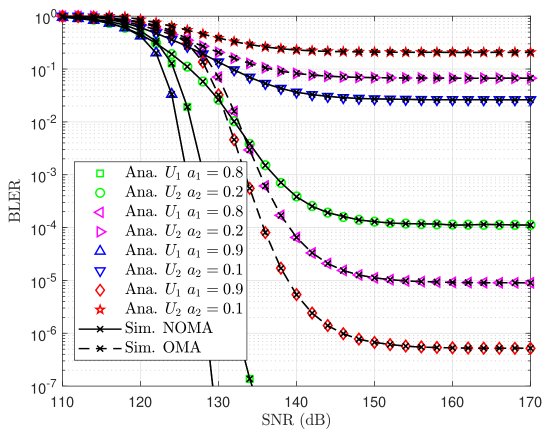

(b)

FIGURE 2. Average BLER with various power allocation coefficients with $\sigma_e^2 = 10^{-13}$ and perfect SIC.

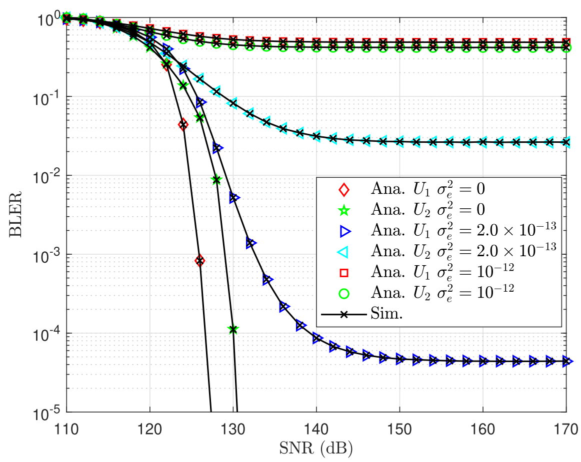

FIGURE 3. The BLER performance of users in the SPC-NOMA VLC system with various values of σ_e^2 and perfect SIC.

scenarios. In addition, the BLER curves in the imperfect CSI scenarios show error floor performance. The error floor effect is presented clearly when the channel estimation error variance increases from 2.0×10^{-13} to 10^{-12}. The error floor occurs since the interference of the channel estimation error in the received SINR increases with the transmitted SNR according to (23), (24), and (25). This shows that the BLER performance decreases with the channel estimation error, as expected.

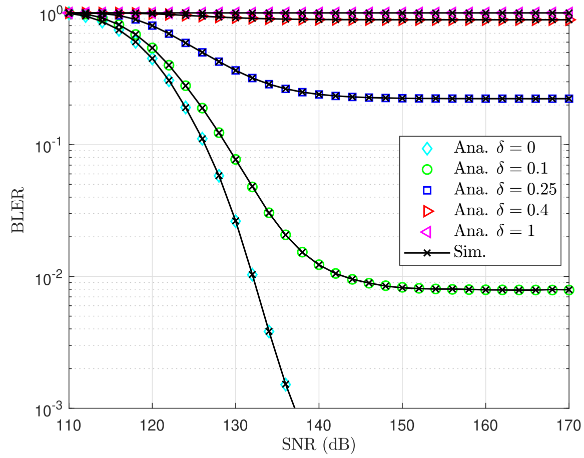

FIGURE 4. The average BLER at U_2 with imperfect SIC, $\sigma_e^2 = 10^{-13}$, and $\delta = 0, 0.1, 0.25, 0.4, 1$.

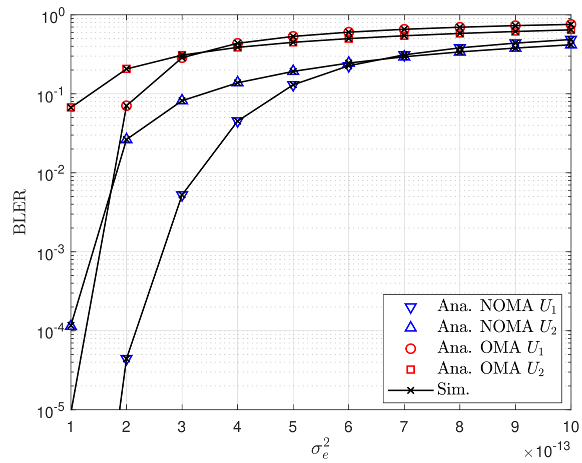

FIGURE 5. The BLER performance of users in the SPC-NOMA system and SPC-OMA system with various values of σ_e^2, $\delta = 0$, and $\gamma_{\text{Tx}} = 160$ dB.

In Fig. 4, we investigate the impact of both imperfect CSI and imperfect SIC on the average BLER at U_2 with a fixed value of σ_e^2 and various values of δ as a function of the transmit SNR. The results show that the BLER performance of U_2 decreases with an increase in the amount of the imperfect SIC. The BLER decreases to the floor error value when the transmit power increases at each value of δ. Moreover, the average BLER performance approaches the floor error value at the lower value of the transmit SNR when the imperfect SIC coefficients increase (i.e., 150 dB with $\delta = 0.1$, 145 dB with $\delta = 0.25$, and 135 dB with $\delta = 0.4$).

Fig. 5 depicts the BLER performance of the SPC-NOMA VLC system versus SPC-OMA VLC system as a function of σ_e^2 at 160 dB. The BLER performances of all users in

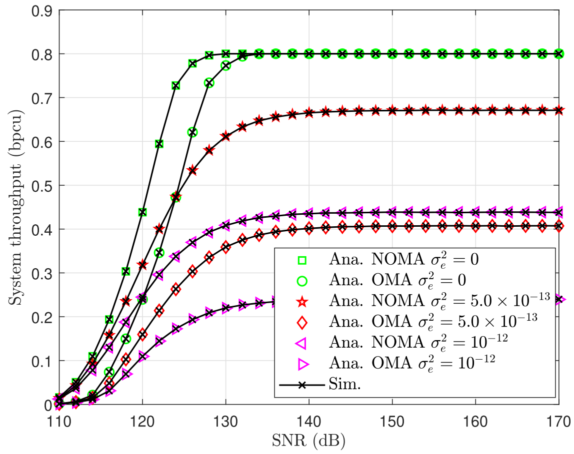

FIGURE 6. The system throughput of the SPC-OMA VLC system versus the SPC-NOMA VLC system for $\delta = 0$.

the SPC-NOMA VLC system are better than those of all users in the SPC-OMA VLC system with various values of σ_e^2. In the SPC-OMA VLC system, the average BLER of U_1 outperforms that of U_2 with $\sigma_e^2 \in [10^{-13}, 3.0 \times 10^{-13}]$, and the average BLER of U_2 is lower than that of U_1 with $\sigma_e^2 \in [3.0 \times 10^{-13}, 10^{-12}]$. In the SPC-NOMA VLC system, the BLER of U_1 outperforms that of U_2 with $\sigma_e^2 \in [10^{-13}, 7.0 \times 10^{-13}]$. However, the BLER of U_2 outperforms that of U_1 with $\sigma_e^2 \in [7 \times 10^{-13}, 10^{-12}]$, since U_1 has lower channel gain, which is sensitive to the channel estimation error. Moreover, U_1 decodes s_1 with the interference of U_2, which increases the impact of the imperfect CSI in decoding messages. However, U_2 has higher channel gain, which is more robust to the channel estimation error. It is concluded that the performance of U_1 in the NOMA system is less sensitive than that of U_1 in the OMA system, and the channel order for the power allocation is not affected significantly by the small channel estimation error.

Fig. 6 illustrates the comparison and impacts of imperfect CSI on the sum throughput of the SPC-OMA VLC system versus the SPC-NOMA VLC system as a function of the SNR for various values of σ_e^2. Firstly, the SPC-NOMA system provides higher throughput than the SPC-OMA system. Furthermore, the system throughput of the SPC-NOMA VLC system in imperfect CSI cases is higher than that of the SPC-OMA VLC system in the perfect CSI case when the SNR is smaller than 120 dB. Secondly, the system throughput decreases when the channel estimation error increases, as expected. For instance, when the channel error increases from 0 to 10^{-12}, the system throughput of the SPC-NOMA VLC system decreases from 0.8 bpcu to 0.44 bpcu, and the system throughput of the SPC-OMA VLC system decreases from 0.8 bpcu to 0.24 bpcu. Hence, the throughput of the SPC-NOMA VLC system is double that of the SPC-OMA VLC system in the imperfect SIC case. Lastly, there exists a ceiling bound of the system throughput for both NOMA and OMA schemes. The OMA scheme reaches the ceiling bound at lower transmit SNR (i.e., 145 dB)

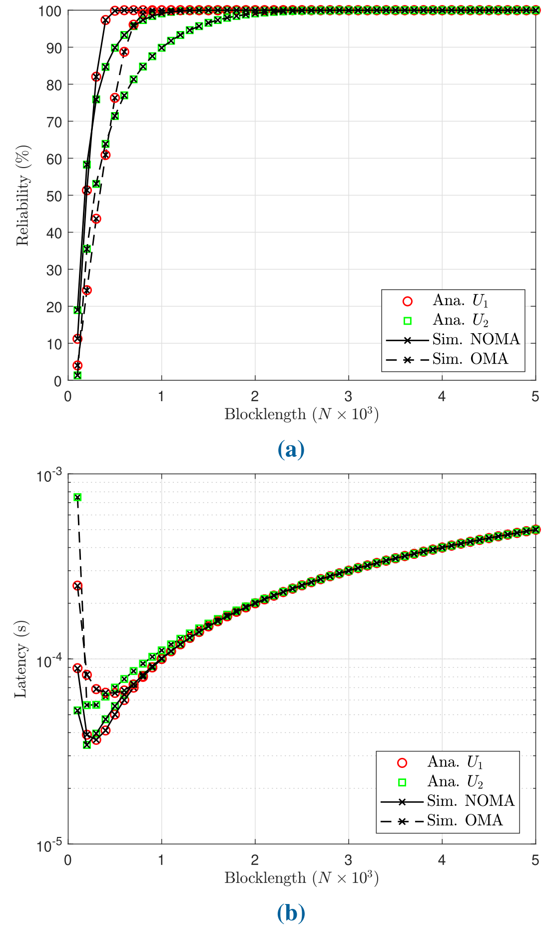

FIGURE 7. Reliability and latency of users in the SPC-OMA VLC system versus the SPC-NOMA VLC system with $\sigma_e^2 = 10^{-12}$, $\gamma_{Tx} = 160$ dB, and $\delta = 0$.

in comparison to the NOMA scheme (i.e., 150 dB). This demonstrates the importance of considering the imperfect CSI in the practical design for the robust operation of the SPC-NOMA VLC system.

Fig. 7 presents the reliability and latency of the SPC-NOMA-VLC system as a function of the block-length N for a fixed value of $\sigma_e^2 = 10^{-12}$. The reliability of the systems can achieve the requirement for ULLC applications. The SPC-OMA VLC system requires a higher number of block-length than the SPC-NOMA VLC system to obtain the required reliability (i.e., 1500 block-length for SPC-NOMA VLC system, and 3000 block-length for the SPC-OMA VLC system). According to (4), the BLER of each user depends on both transmit SNR and transmission rate, where the BLER is an increasing function with respect to the transmission rate. The SPC-NOMA VLC system simultaneously supports two users by using the same number of block-length ($N_1 = N_2 = N$), while the SPC-OMA VLC system supports two users separately, and the block-length for each user should be half of that for each user in the NOMA system (i.e., $N_1 = N_2 = N/2$). Consequently, the NOMA system provides higher reliability than the OMA system. With the channel estimation error, the latency of both NOMA and OMA

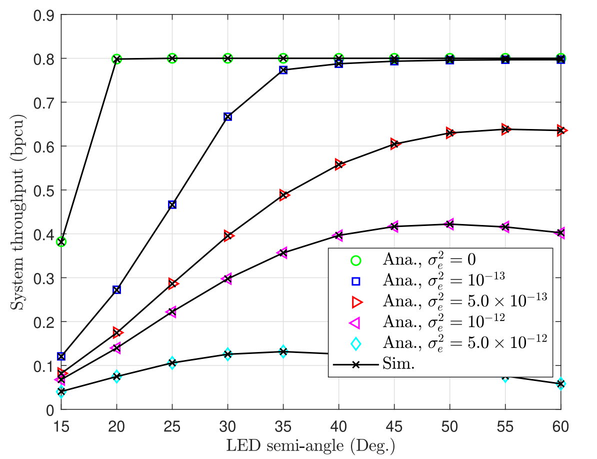

FIGURE 8. System throughput versus LED semi-angle in SPC-NOMA VLC system at different values of σ_e^2 and $\delta = 0.1$.

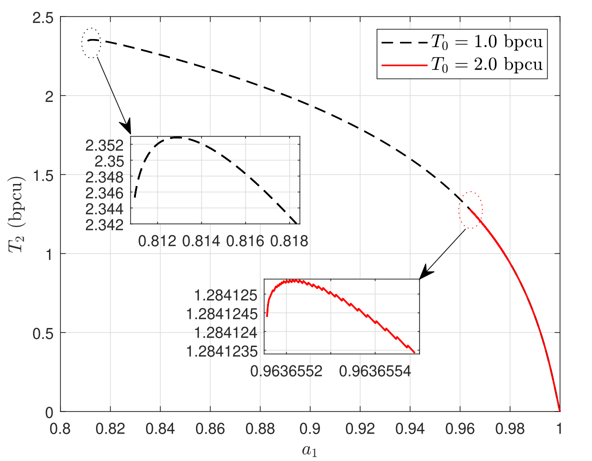

FIGURE 9. The achievable throughput T_2 in the SPC-NOMA VLC system with various values of T_0 with respect to a_1 when $\sigma_e^2 = 2.0 \times 10^{-13}$, $\gamma_{Tx} = 160$ dB, $\hat{h}_1 = 4.0 \times 10^{-6}$ and $\hat{h}_2 = 6.0 \times 10^{-6}$.

systems satisfies the requirement of URLLC applications (delay in sub-milli second). Moreover, the latency of the NOMA VLC system is half of that of the OMA VLC system. This indicates that there exists a trade-off between reliability and latency when increasing the block-length to increase reliability of users in the system.

Fig. 8 demonstrates the system throughput as a function of the LED semi-angle in the SPC-NOMA VLC system with different values of σ_e^2. The maximum system throughput decreases from 0.8 bpcu in the perfect CSI case to 0.13 bpcu in the imperfect CSI case (i.e., $\sigma_e^2 = 5.0 \times 10^{-12}$). When the channel estimation error increases from 0 to 10^{-13}, the LED with high semi-angle can provide maximum throughput. In contrast, when the channel estimation error increases from 5.0×10^{-13} to 5.0×10^{-12}, the channel gains are less distinctive. Therefore, the LED with lower semi-angle can provide maximum throughput. The higher LED semi-angle can provide maximum system throughput with σ_e^2 less than 5.0×10^{-13}.

Fig. 9 depicts the achieved effective throughput T_2 as a function of a_1 where a_2, R_1 and R_2 are optimized according to steps in the optimal design, and $\hat{h}_1$ and $\hat{h}_2$ are fixed values. From Fig. 9, there exists the lower bound of the power allocation for U_1 to provide the effective throughput T_0 at U_2, denoted by a_1^b. The result shows that a_1^b increases with T_0. The effective throughput T_2 is set to 0 when a_1 is less than a_1^b. Moreover, the maximum effective throughput T_2 cannot be derived at a_1^b due to the relationship in expressions of BLER in (60) and (64). Therefore, it indicates that T_2 is not an increasing function with a_2.

VI. CONCLUSION

We investigate the imperfect CSI and imperfect SIC in the SPC-NOMA VLC system. The performance of the SPC-NOMA VLC system decreases with the presence of the imperfect CSI. The BLER performance of the far user is degraded with imperfect SIC, as expected. The closed-form expressions of the analytical results are verified by Monte Carlo simulations. The performance of the SPC-NOMA VLC system with perfect SIC is compared to that of the SPC-OMA VLC system in terms of BLER, reliability, latency, and throughput. The results show that the SPC-NOMA VLC system outperforms the SPC-OMA VLC system. Moreover, we propose a simple method to maximize the effective throughput of the near users while guaranteeing a certain effective throughput for far users. This work is envisaged to be useful for the theoretical and practical design of VLC-based systems with low latency such as factory automation and intelligent transport systems.

APPENDIX A PROOF OF LEMMA 1

From (4) and (55), we have

$$T_1 = R_1 \left(1 - Q\left(f\left(\hat{\gamma}_{11}, R_1, N\right)\right)\right). \tag{68}$$

To know the monotonicity of T_1 with respect to R_1, we examine the first derivative of T_1 with respect to R_1, expressed by

$$\begin{aligned}\frac{\partial T_1}{\partial R_1} &= 1 - Q\left(f\left(\hat{\gamma}_{11}, R_1, N\right)\right) \\ &\quad - R_1 \frac{1}{\sqrt{2\pi}} \Theta\left(\hat{\gamma}_{11}\right) e^{-\frac{1}{2} f^2\left(\hat{\gamma}_{11}, R_1, N\right)},\end{aligned} \tag{69}$$

where $\Theta\left(\hat{\gamma}_i\right) = \frac{2}{\log_2 e \sqrt{2\left(1-\left(1+\hat{\gamma}_i\right)^{-2}\right)/N}}$. (69) indicates that the first derivative of T_1 with respect to R_1 is not always positive or negative. Therefore, T_1 is not an increasing or decreasing function with R_1.

We examine the concavity of T_1 with R_1. The second derivative of T_1 with respect to R_1 is given by

$$\begin{aligned}\frac{\partial^2 T_1}{\partial R_1^2} &= -\frac{2}{\sqrt{2\pi}} \Theta\left(\hat{\gamma}_{11}\right) e^{-\frac{1}{2} f^2\left(\hat{\gamma}_{11}, R_1, N\right)} \\ &\quad - R_1 \frac{1}{\sqrt{2\pi}} f\left(\hat{\gamma}_{11}, R_1, N\right) \Theta^2\left(\hat{\gamma}_{11}\right) e^{-\frac{1}{2} f^2\left(\hat{\gamma}_{11}, R_1, N\right)}.\end{aligned} \tag{70}$$

Since $\frac{\partial^2 T_1}{\partial R_1^2} \leq 0$, T_1 is the concave function with R_1.

APPENDIX B PROOF OF PROPOSITION 3

According to [35, Chapter 1], the condition for the iteration convergence is $\left|\frac{\partial\mathcal{T}(R_1)}{\partial R_1}\right| < 1$. This condition is satisfied with $R_1 \in [0, R_1^{\text{opt}}]$, where $T_1'(R_1^{\text{opt}}) = 0$. To clarify the convergence, we examine the monotonicity of $\mathcal{T}(R_1)$ with R_1. From (69), the first derivative of $\mathcal{T}(R_1)$ with R_1 is written as

$$\frac{\partial\mathcal{T}(R_1)}{\partial R_1} = \frac{\Theta\left(\hat{\gamma}_{11}\right)e^{-\frac{1}{2}f^2(\hat{\gamma}_{11},R_1,N)}}{\sqrt{2\pi}} \times \frac{T_0}{\left(1-Q\left(f\left(\gamma_{11},R_1,N\right)\right)\right)^2}. \tag{71}$$

The second derivative of $\mathcal{T}(R_1)$ with R_1 is expressed by

$$\frac{\partial^2\mathcal{T}(R_1)}{\partial R_1^2} = \frac{\Theta^2\left(\hat{\gamma}_{11}\right)T_0}{\sqrt{2\pi}} \times \left(\frac{f\left(\hat{\gamma}_{11},R_1,N\right)e^{-\frac{1}{2}f^2(\gamma_{11},R_1,N)}}{\left(1-Q\left(f\left(\hat{\gamma}_{11},R_1,N\right)\right)\right)^2} + \frac{2e^{-f^2(\hat{\gamma}_{11},R_1,N)}}{\sqrt{2\pi}\left(1-Q\left(f\left(\hat{\gamma}_{11},R_1,N\right)\right)\right)^3}\right). \tag{72}$$

Since $\Theta\left(\hat{\gamma}_{11}\right) \geq 0$ and $f\left(\hat{\gamma}_{11},R_1,N\right) \geq 0$, $\frac{\partial^2\mathcal{T}(R_1)}{\partial R_1^2} \geq 0$. $\frac{\partial\mathcal{T}(R_1)}{\partial R_1}$ is an increasing function with R_1. Due to $R_1 \in [0, R_1^{\text{opt}}]$, we investigate the value of $\frac{\partial\mathcal{T}(R_1)}{\partial R_1}$ at R_1^{opt}. From (69), since $T_1'\left(R_1^{\text{opt}}\right) = 0$, we have

$$1-Q\left(f\left(\hat{\gamma}_{11},R_1^{\text{opt}},N\right)\right) = R_1\frac{1}{\sqrt{2\pi}}\Theta\left(\hat{\gamma}_{11}\right)e^{-\frac{1}{2}f^2\left(\hat{\gamma}_{11},R_1^{\text{opt}},N\right)}. \tag{73}$$

Substituting (73) into (71), we obtain

$$\frac{\partial\mathcal{T}\left(R_1^{\text{opt}}\right)}{\partial R_1^{\text{opt}}} = \frac{T_0}{R_1^{\text{opt}}\left(1-Q\left(f\left(\hat{\gamma}_{11},R_1^{\text{opt}},N\right)\right)\right)}. \tag{74}$$

Since $R_1^{\text{opt}}\left(1-Q\left(f\left(\hat{\gamma}_{11},R_1^{\text{opt}},N\right)\right)\right) \geq T_0$, $\left|\frac{\partial\mathcal{T}(R_1)}{\partial R_1}\right| < 1$ with $R_1 \in [0, R_1^{\text{opt}}]$.

APPENDIX C PROOF OF LEMMA 2

Since the channel in the VLC system is real value, the transmission rate of the finite block-length transmission with a given error probability ε_i at U_i is approximated by [7]

$$R_i = 0.5\log_2\left(1+\gamma_i\right) - \sqrt{\frac{1-\left(1+\gamma_i\right)^{-2}}{2N_i}}\frac{Q^{-1}\left(\varepsilon_i\right)}{\ln 2}, \tag{75}$$

where $Q^{-1}(.)$ is the inverse Q-function. Therefore, the boundary of the transmission rate in finite block-length transmission at U_i is $0 \leq R_i \leq 0.5\log_2\left(1+\gamma_i\right)$.

If SIC is imperfect and $0 \leq R_2 \leq 0.5\log_2\left(1+\hat{\gamma}_{22}'\right)$, the throughput at U_2 with the conditioned R_2 is written as

$$T_2' = R_2\left(\left(1-Q\left(f\left(\hat{\gamma}_{22},R_2,N\right)\right)\right)\left(1-\varepsilon_{21}\right) + \varepsilon_{21}\left(1-Q\left(f\left(\hat{\gamma}_{22}',R_2,N\right)\right)\right)\right). \tag{76}$$

We investigate the monotonicity and concavity of T_2' with respect to R_2. The first derivative of T_2' with respect to R_2 is given by

$$\frac{\partial T_2'}{\partial R_2} = \left(1-Q\left(f\left(\hat{\gamma}_{22},R_2,N\right)\right) - \frac{1}{\sqrt{2\pi}}R_2\Theta\left(\hat{\gamma}_{22}\right)e^{-\frac{1}{2}f^2(\hat{\gamma}_{22},R_2,N)}\right)\left(1-\varepsilon_{21}\right) + \varepsilon_{21}\left(1-Q\left(f\left(\hat{\gamma}_{22}',R_2,N\right)\right) - \frac{1}{\sqrt{2\pi}}R_2\Theta\left(\hat{\gamma}_{22}'\right)e^{-\frac{1}{2}f^2(\hat{\gamma}_{22}',R_2,N)}\right). \tag{77}$$

(77) indicates that T_2' does not always increase with respect to R_2. The second derivative of T_2' with respect to R_2 is written as

$$\frac{\partial^2 T_2'}{\partial R_2^2} = -\left(\frac{2}{\sqrt{2\pi}}\Theta\left(\hat{\gamma}_{22}\right)e^{-\frac{1}{2}f^2(\hat{\gamma}_{22},R_2,N)} + \frac{1}{\sqrt{2\pi}}R_2\Theta^2\left(\hat{\gamma}_{22}\right)f\left(\hat{\gamma}_{22},R_2,N\right)e^{-\frac{1}{2}f^2(\hat{\gamma}_{22},R_2,N)}\right) \times \left(1-\varepsilon_{21}\right) - \left(\frac{2}{\sqrt{2\pi}}\Theta\left(\hat{\gamma}_{22}'\right)e^{-\frac{1}{2}f^2(\hat{\gamma}_{22}',R_2,N)} + \frac{1}{\sqrt{2\pi}}R_2\Theta^2\left(\hat{\gamma}_{22}'\right)f\left(\hat{\gamma}_{22}',R_2,N\right)e^{-\frac{1}{2}f^2(\hat{\gamma}_{22}',R_2,N)}\right)\varepsilon_{21}. \tag{78}$$

From (78), we have $\frac{\partial^2 T_2'}{\partial R_2^2} \leq 0$. T_2' is a concave function with respect to R_2.

If SIC is perfect and $0.5\log_2\left(1+\hat{\gamma}_{22}'\right) \leq R_2 \leq 0.5\log_2\left(1+\hat{\gamma}_{22}\right)$, the throughput at U_2 with the conditioned R_2 is given by

$$T_2 = R_2\left(1-\varepsilon_{21}\right)\left(1-Q\left(f\left(\hat{\gamma}_{22},R_2,N\right)\right)\right). \tag{79}$$

We examine the monotonicity and concavity of T_2 with respect to R_2. The first derivative of T_2 with respect to R_2 is given by

$$\frac{\partial T_2}{\partial R_2} = \left(1-\varepsilon_{21}\right)\left(1-Q\left(f\left(\hat{\gamma}_{22},R_2,N\right)\right) - R_2\frac{1}{\sqrt{2\pi}}\Theta\left(\hat{\gamma}_{22}\right)e^{-\frac{1}{2}f^2(\hat{\gamma}_{22},R_2,N)}\right). \tag{80}$$

T_2 is not an increasing function with R_2. The second derivative of T_2 with R_2 is given by

$$\frac{\partial^2 T_2}{\partial R_2^2} = \left(1-\varepsilon_{21}\right)\left(-\frac{2}{\sqrt{2\pi}}\Theta\left(\hat{\gamma}_{22}\right)e^{-\frac{1}{2}f^2(\hat{\gamma}_{22},R_2,N)} - R_2 \times \frac{1}{\sqrt{2\pi}}\Theta^2\left(\hat{\gamma}_{22}\right)f\left(\hat{\gamma}_{22},R_2,N\right)e^{-\frac{1}{2}f^2(\hat{\gamma}_{22},R_2,N)}\right). \tag{81}$$

T_2 is concave function with R_2. Therefore, the effective throughput at U_2 is a concave function in the feasible range of R_2.

REFERENCES

[1] T. Asai, "5G radio access network and its requirements on mobile optical network," in *Proc. Int. Conf. Opt. Netw. Design Modeling (ONDM)*, May 2015, pp. 7–11.

[2] J. G. Andrews, S. Buzzi, W. Choi, S. V. Hanly, A. Lozano, A. C. K. Soong, and J. C. Zhang, "What will 5G be?" *IEEE J. Sel. Areas Commun.*, vol. 32, no. 6, pp. 1065–1082, Jun. 2014.

[3] S. Dimitrov and H. Haas, *Principles of LED Light Communications: Towards Networked Li-Fi*. Cambridge, U.K.: Cambridge Univ. Press, Mar. 2015.

[4] G. J. Sutton, J. Zeng, R. P. Liu, W. Ni, D. N. Nguyen, B. A. Jayawickrama, X. Huang, M. Abolhasan, Z. Zhang, E. Dutkiewicz, and T. Lv, "Enabling technologies for ultra-reliable and low latency communications: From PHY and MAC layer perspectives," *IEEE Commun. Surveys Tuts.*, vol. 21, no. 3, pp. 2488–2524, 3rd Quart., 2019.

[5] O. N. C. Yilmaz, Y.-P.-E. Wang, N. A. Johansson, N. Brahmi, S. A. Ashraf, and J. Sachs, "Analysis of ultra-reliable and low-latency 5G communication for a factory automation use case," in *Proc. IEEE Int. Conf. Commun. Workshop (ICCW)*, London, U.K., Jun. 2015, pp. 1190–1195.

[6] G. Durisi, T. Koch, and P. Popovski, "Toward massive, ultrareliable, and low-latency wireless communication with short packets," *Proc. IEEE*, vol. 104, no. 9, pp. 1711–1726, Sep. 2016.

[7] Y. Polyanskiy, H. V. Poor, and S. Verdu, "Channel coding rate in the finite blocklength regime," *IEEE Trans. Inf. Theory*, vol. 56, no. 5, pp. 2307–2359, May 2010.

[8] W. Yang, G. Durisi, T. Koch, and Y. Polyanskiy, "Quasi-static multiple-antenna fading channels at finite blocklength," *IEEE Trans. Inf. Theory*, vol. 60, no. 7, pp. 4232–4265, Jul. 2014.

[9] S. I. Bross, A. Lapidoth, and S. Tinguely, "Broadcasting correlated Gaussians," *IEEE Trans. Inf. Theory*, vol. 56, no. 7, pp. 3057–3068, Jul. 2010.

[10] M. Shirvanimoghaddam, M. S. Mohammadi, R. Abbas, A. Minja, C. Yue, B. Matuz, G. Han, Z. Lin, W. Liu, Y. Li, S. Johnson, and B. Vucetic, "Short block-length codes for ultra-reliable low latency communications," *IEEE Commun. Mag.*, vol. 57, no. 2, pp. 130–137, Feb. 2019.

[11] A. Lapidoth and S. Tinguely, "Sending a bivariate Gaussian over a Gaussian MAC," *IEEE Trans. Inf. Theory*, vol. 56, no. 6, pp. 2714–2752, Jun. 2010.

[12] H. Wang, Q. Yang, Z. Ding, and H. V. Poor, "Secure short-packet communications for mission-critical IoT applications," *IEEE Trans. Wireless Commun.*, vol. 18, no. 5, pp. 2565–2578, May 2019.

[13] B. Makki, T. Svensson, and M. Zorzi, "Finite block-length analysis of spectrum sharing networks using rate adaptation," *IEEE Trans. Commun.*, vol. 63, no. 8, pp. 2823–2835, Aug. 2015.

[14] W. Yang, G. Caire, G. Durisi, and Y. Polyanskiy, "Optimum power control at finite blocklength," *IEEE Trans. Inf. Theory*, vol. 61, no. 9, pp. 4598–4615, Sep. 2015.

[15] S. Xu, T.-H. Chang, S.-C. Lin, C. Shen, and G. Zhu, "Energy-efficient packet scheduling with finite blocklength codes: Convexity analysis and efficient algorithms," *IEEE Trans. Wireless Commun.*, vol. 15, no. 8, pp. 5527–5540, Aug. 2016.

[16] I. Budhiraja, N. Kumar, S. Tyagi, S. Tanwar, Z. Han, M. J. Piran, and D. Y. Suh, "A systematic review on NOMA variants for 5G and beyond," *IEEE Access*, vol. 9, pp. 85573–85644, 2021.

[17] K. Chung, "NOMA for correlated information sources in 5G systems," *IEEE Commun. Lett.*, vol. 25, no. 2, pp. 422–426, Feb. 2021.

[18] Z. Wang, Z. Lin, T. Lv, and W. Ni, "Energy-efficient resource allocation in massive MIMO-NOMA networks with wireless power transfer: A distributed ADMM approach," *IEEE Internet Things J.*, vol. 8, no. 18, pp. 14232–14247, Sep. 2021.

[19] Z. Ding, F. Adachi, and H. V. Poor, "The application of MIMO to non-orthogonal multiple access," *IEEE Trans. Wireless Commun.*, vol. 15, no. 1, pp. 537–552, Jan. 2016.

[20] J. Men and J. Ge, "Non-orthogonal multiple access for multiple-antenna relaying networks," *IEEE Commun. Lett.*, vol. 19, no. 10, pp. 1686–1689, Oct. 2015.

[21] Y. Song, W. Yang, Z. Xiang, N. Sha, H. Wang, and Y. Yang, "An analysis on secure millimeter wave NOMA communications in cognitive radio networks," *IEEE Access*, vol. 8, pp. 78965–78978, 2020.

[22] H. Marshoud, V. M. Kapinas, G. K. Karagiannidis, and S. Muhaidat, "Non-orthogonal multiple access for visible light communications," *IEEE Photon. Technol. Lett.*, vol. 28, no. 1, pp. 51–54, Jan. 1, 2016.

[23] L. Yin, W. O. Popoola, X. Wu, and H. Haas, "Performance evaluation of non-orthogonal multiple access in visible light communication," *IEEE Trans. Commun.*, vol. 64, no. 12, pp. 5162–5175, Dec. 2016.

[24] H. Marshoud, P. C. Sofotasios, S. Muhaidat, G. K. Karagiannidis, and B. S. Sharif, "On the performance of visible light communication systems with non-orthogonal multiple access," *IEEE Trans. Wireless Commun.*, vol. 16, no. 10, pp. 6350–6364, Oct. 2017.

[25] C. Chen, W.-D. Zhong, H. Yang, and P. Du, "On the performance of MIMO-NOMA-based visible light communication systems," *IEEE Photon. Technol. Lett.*, vol. 30, no. 4, pp. 307–310, Feb. 15, 2018.

[26] G. N. Tran and S. Kim, "Performance analysis of short packets in NOMA VLC systems," *IEEE Access*, vol. 10, pp. 6505–6517, 2022.

[27] M. B. Janjua, D. B. da Costa, and H. Arslan, "User pairing and power allocation strategies for 3D VLC-NOMA systems," *IEEE Wireless Commun. Lett.*, vol. 9, no. 6, pp. 866–870, Jun. 2020.

[28] C. Du, F. Zhang, S. Ma, Y. Tang, H. Li, H. Wang, and S. Li, "Secure transmission for downlink NOMA visible light communication networks," *IEEE Access*, vol. 7, pp. 65332–65341, 2019.

[29] *Study on Downlink Multiuser Superposition Transmission for LTE*, 3GPP, Shanghai, China, Mar. 2015.

[30] D. J. F. Barros, S. K. Wilson, and J. M. Kahn, "Comparison of orthogonal frequency-division multiplexing and pulse-amplitude modulation in indoor optical wireless links," *IEEE Trans. Commun.*, vol. 60, no. 1, pp. 153–163, Jan. 2012.

[31] H. A. David and H. N. Nagaraja, *Order Statistics*, 3rd ed. New York, NY, USA: Wiley, 2003.

[32] A. Al Hammadi, P. C. Sofotasios, S. Muhaidat, M. Al-Qutayri, and H. Elgala, "Non-orthogonal multiple access for hybrid VLC-RF networks with imperfect channel state information," *IEEE Trans. Veh. Technol.*, vol. 70, no. 1, pp. 398–411, Jan. 2021.

[33] M. Abramowitz and I. A. Stegun, Eds., *Handbook of Mathematical Functions with Formulas, Graphs, and Mathematical Tables*, 9th ed. Washington, DC, USA: U.S. Government Printing Office, 1972.

[34] H. Ren, C. Pan, Y. Deng, M. Elkashlan, and A. Nallanathan, "Joint power and blocklength optimization for URLLC in a factory automation scenario," *IEEE Trans. Wireless Commun.*, vol. 19, no. 3, pp. 1786–1801, Mar. 2020.

[35] E. Suli and D. F. Mayers, *An Introduction to Numerical Analysis*. Cambridge, U.K.: Cambridge Univ. Press, 2003.

[36] K. Sikorski and H. Wozniakowski, "Complexity of fixed points, I," *J. Complex.*, vol. 3, no. 4, pp. 388–405, Dec. 1987.

[37] S. Gong, S. Ma, C. Xing, and G. Yang, "Optimal beamforming and time allocation for partially wireless powered sensor networks with downlink SWIPT," *IEEE Trans. Signal Process.*, vol. 67, no. 12, pp. 3197–3212, Jun. 2019.

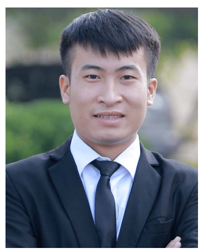

GIANG N. TRAN (Graduate Student Member, IEEE) received the B.S. degree from the Advanced Program in Electrical Engineering, Thai Nguyen University of Technology, Vietnam, in 2019. He is currently pursuing the M.S. and Ph.D. combined degree with the Department of Electrical, Electronic and Computer Engineering, University of Ulsan, South Korea. His main research interests include ultra-reliable and low-latency communication, 5G communication, and visible light communication.

SUNGHWAN KIM (Member, IEEE) received the B.S., M.S., and Ph.D. degrees from Seoul National University, South Korea, in 1999, 2001, and 2005, respectively. He was a Postdoctoral Visitor at the Georgia Institute of Technology (GeorgiaTech), from 2005 to 2007, and a Senior Engineer at Samsung Electronics, from 2007 to 2011. He is currently a Professor at the Department of Electrical, Electronic and Computer Engineering, University of Ulsan, South Korea. His main research interests include channel coding, modulation, massive MIMO, visible light communication, quantum information, and storage systems.